

# Fabrication of Microlens Arrays with High Quality and High Fill Factor by Inkjet Printing

Qiaoshuang Zhang,\* Maximilian Schambach, Stefan Schliske, Qihao Jin, Adrian Mertens, Christian Rainer, Gerardo Hernandez-Sosa, Michael Heizmann, and Uli Lemmer\*

Microlens arrays (MLAs) have a variety of applications in, e.g., display systems, projection optics, and sensors. They can be manufactured by various fabrication methods. Among all, inkjet printing stands out because it offers a straightforward, versatile, and low-cost fabrication route. However, extra manufacturing steps such as photolithography are so far involved to pre-structure the substrate in order to improve the uniformity of the printed MLAs and achieve a high fill factor (FF). In this study, the fabrication of MLAs is reported on unstructured substrates by inkjet printing using an optimized UV-curable ink on top of self-assembled monolayers (SAMs). The latter allows for tuning the surface free energy and thus the aspect ratio of the microlenses. The high uniformity of the printed MLAs is demonstrated by the automatic quantitative evaluations, where the standard deviations of the radii are below 2.5% and of the sag heights are less than 3.9%. An unprecedented FF of 88% amongst all inkjet-printed MLAs on unstructured substrates is achieved. Digitally controlled large area fabrication is demonstrated, both, on rigid as well as on flexible substrates, opening a pathway for customized microoptics by additive manufacturing.

## 1. Introduction

A microlens array (MLA) is an essential miniaturized component in micro-optical systems due to its advantages of high compactness and integration, small size, and designable optical properties.<sup>[1]</sup> With the ability to shape, focus, and diffuse a light beam, MLAs have been widely used in various applications such as light-emitting diodes (LEDs),<sup>[2]</sup> sensors,<sup>[3]</sup> solar cells,<sup>[4]</sup> light field cameras,<sup>[5]</sup> anticounterfeiting,<sup>[6]</sup> lithography,<sup>[7]</sup> and lasers.<sup>[8]</sup> In these devices and systems, MLAs with a high fill factor (FF) are key to boosting the light collection/extraction efficiency or improving imaging resolution.<sup>[9]</sup>

Different fabrication methods have been developed to fabricate high-FF MLAs. One approach is the thermal reflow method, where an MLA is obtained by applying heat to reshape a micro-disc array previously fabricated by lithography<sup>[10]</sup> and laser catapulting.<sup>[11]</sup> Compared to the photolithographic process, which involves multiple fabrication steps and relies on the photomasks, laser catapulting is a technique that allows for rapid and maskless manufacturing. However, the thermal reflow process requires high temperatures, and it is challenging to fabricate microlenses (MLs) with high numerical apertures (NA).<sup>[12]</sup> Other approaches, including hot embossing,<sup>[13]</sup> electrowetting,<sup>[14]</sup> and soft lithography<sup>[15]</sup> have been adopted to fabricate MLAs with a FF of nearly 100%. However, these approaches do not allow for additive manufacturing on various substrates and fast prototyping of MLAs.

Alternatively, direct laser writing as an additive manufacturing technology enables the maskless fabrication of high-FF MLAs with high precision.<sup>[16]</sup> However, the need for systems with high complexity and ultrafast lasers leads to high costs, and the sequential voxel-by-voxel method has limitations in the throughput. In contrast, inkjet printing, which also allows for maskless additive manufacturing of MLAs, offers a variety of advantages.<sup>[12,17]</sup> First, inkjet printing is a straightforward and versatile process where the fabrication of MLAs is digitally controlled in a real-time manner, which allows for fast prototyping of MLAs. Second, only the material amount needed for the MLs is used in printing, thereby preventing the material waste to a large extent and improving the cost-effectiveness. In addition, inkjet printing is a non-contact technique, and the printing

Q. Zhang, S. Schliske, Q. Jin, A. Mertens, C. Rainer,  
G. Hernandez-Sosa, U. Lemmer  
Light Technology Institute  
Karlsruhe Institute of Technology (KIT)  
Engesserstrasse 13, 76131 Karlsruhe, Germany  
E-mail: qiaoshuang.zhang@kit.edu; uli.lemmer@kit.edu

M. Schambach, M. Heizmann  
Institute of Industrial Information Technology  
Karlsruhe Institute of Technology (KIT)  
Hertzstrasse 16, 76187 Karlsruhe, Germany

S. Schliske, C. Rainer, G. Hernandez-Sosa, U. Lemmer  
InnovationLab

Speyerer Strasse 4, 69115 Heidelberg, Germany

A. Mertens, G. Hernandez-Sosa, U. Lemmer  
Institute of Microstructure Technology  
Karlsruhe Institute of Technology (KIT)  
Hermann-von-Helmholtz-Platz 1  
76344 Eggenstein-Leopoldshafen, Germany

 The ORCID identification number(s) for the author(s) of this article can be found under <https://doi.org/10.1002/adom.202200677>.

© 2022 The Authors. Advanced Optical Materials published by Wiley-VCH GmbH. This is an open access article under the terms of the Creative Commons Attribution-NonCommercial-NoDerivs License, which permits use and distribution in any medium, provided the original work is properly cited, the use is non-commercial and no modifications or adaptations are made.

DOI: 10.1002/adom.202200677

process can be easily transferred to different substrates. Last but not least, the inkjet printing process is capable of upscaling by applying more nozzles or multiple printheads and therefore enabling high throughput and mass production of MLAs.

However, obtaining MLAs with a high FF by inkjet printing is very challenging. Usually, a slight deviation in the positioning of the ink droplets leads to the merging of adjacent droplets, which impedes the quality of the MLAs. Besides, the volume shrinkage of the MLs due to solvent evaporation and curing results in a lower FF. It is possible to fabricate MLAs on unstructured substrates by inkjet printing, but only low uniformity and low FF have been achieved.<sup>[18]</sup> And the FF realized so far is much below the upper limit of a square-aligned circular MLA of 78.5%. To improve the uniformity and the FF of the inkjet-printed MLAs, substrates are usually required to be pre-structured to confine the jetted droplets spatially.<sup>[19]</sup> However, introducing the pre-structuring process, for example, via photolithography, significantly increases the complexity of the whole fabrication process, and the drawbacks outweigh the advantages of using inkjet printing. Until now, a suitable ink and a reliable printing process were yet to be developed to enable the fabrication of high-FF MLAs by inkjet printing.

To the best of our knowledge, we here demonstrate MLAs with unprecedented quality and a high FF of 88%, which has not been previously achieved by inkjet printing without surface structuring steps. The developed UV-curable ink and printing

process improved the position accuracy of the MLs in the array to a large extent. Moreover, the printed MLAs showed a high uniformity, where the standard deviation in ML radii was less than 2.5% and in sag height, it was less than 3.9%. Different NAs of MLAs were achieved by using different self-assembled monolayers (SAMs), showing the possibility of a continuous tuning of the NA. Closely-packed MLAs in a hexagonal layout were printed, where the high FF of 88% was realized by the extremely low shrinkage of our UV-curable ink and the instant in situ UV curing. With the developed ink and printing process, we show the possibility to vastly reduce the fabricating costs and process complexity while maintaining the FF of MLA at a high level.

## 2. Results and Discussion

### 2.1. Ink Formulation and Fabrication of the Tunable MLAs

The schematic of the MLA inkjet printing is shown in Figure 1a. The drop-on-demand (DOD) inkjet printer ejects droplets at specific spots on the substrate. The liquid droplets form a spherical lens shape due to the surface tension, and an MLA is fabricated in this way. SU-8 was chosen as the ink material due to its high transmittance above 360 nm wavelength and high chemical resistance.<sup>[20]</sup> In order to adjust the viscosity of

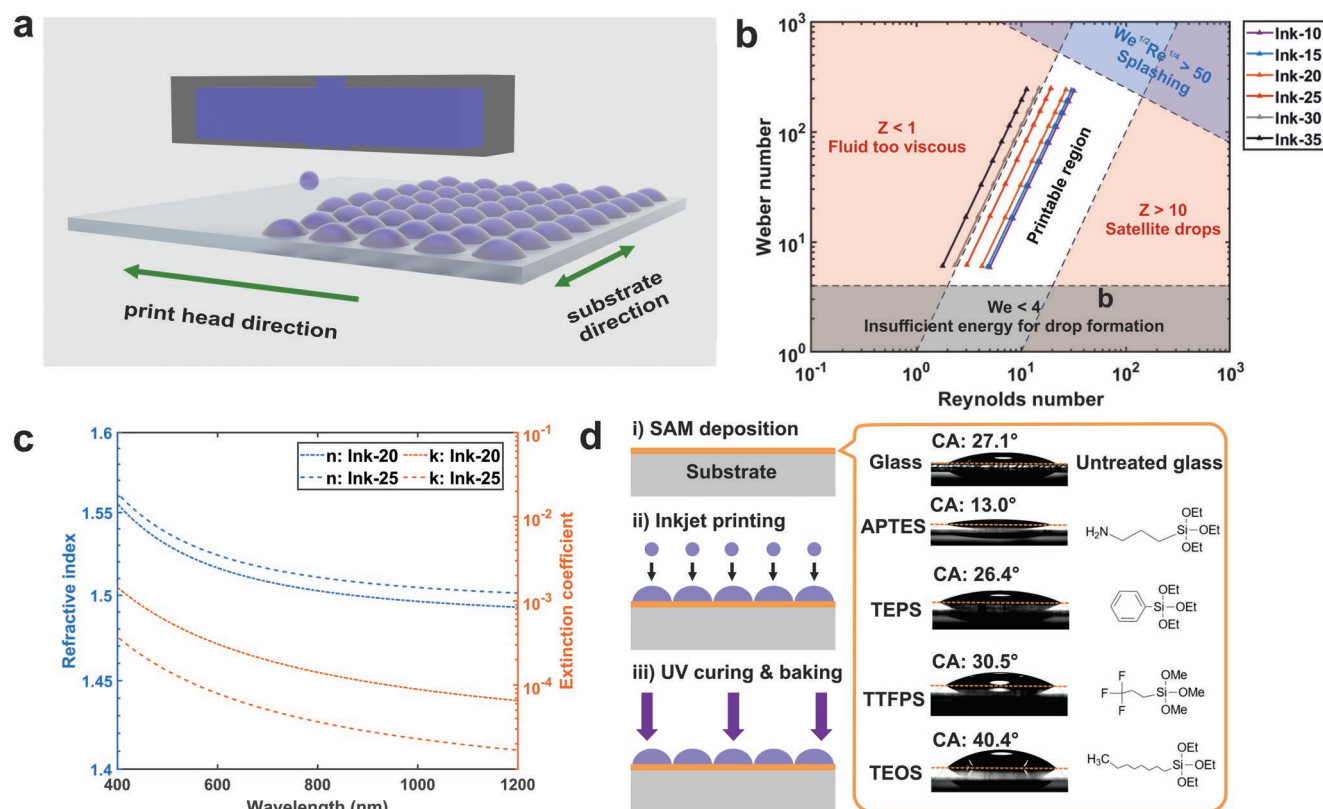


**Figure 1.** a) The schematic of the MLA inkjet printing process. b) The jettability window in Re–We coordinated system. Each solid line represents an ink with different velocities. The white area indicates the printable window. c) The refractive indices (blue lines) and extinction coefficients (orange lines) of thin films printed with Ink-20 and Ink-25, measured by ellipsometry. d) Left side: the fabrication process of printed MLAs. Right side: different CAs of the ink on the substrates treated with different silanes. Orange dashed lines: top surfaces of the substrates.

the ink to the suitable range for inkjet printing, diluents have to be added to the ink. Here, a reactive diluent was added to the ink to circumvent drying effects like the coffee-stain effect caused by the solvent evaporation, as shown in Figure S1, Supporting Information. The FF of an MLA is defined as the ratio of the area covered by MLs to the total area of the array. In order to achieve a high FF by inkjet printing, it is necessary to minimize the shrinkage ratio of the MLs after UV curing and post-exposure bake. Therefore, SU-8 2150, with the highest solid concentration among all SU-8 products, was used as the main component in ink. The reactive diluent Erisys GE-20, which cross-links with SU-8 molecules under UV exposure, was used to decrease the ink's viscosity to achieve a suitable viscosity for inkjet printing while maintaining a small volume shrinkage ratio, as shown in Movie S1 and Figures S2 and S3, Supporting Information. To obtain MLAs with uniform shapes, it is necessary for the droplets ejected from the printer to have the desired shape where no satellite droplets were formed. Here, the satellite-free droplet formation was realized using the developed ink and a customized waveform, and the side view of a droplet can be seen in Figure S4, Supporting Information.

In order to find the optimal ratio between SU-8 and the reactive diluent, inks with different SU-8 concentrations were prepared. The rheological properties of these inks are listed in **Table 1**. As can be seen from Table 1, when the concentration of SU-8 increases from 10% to 35%, the viscosity increases significantly from 13.96 ( $\pm 0.16$ ) mPa·s to 40.15 ( $\pm 0.09$ ) mPa·s at 40 °C (maximum print head temperature). At the same time, there is a very slight variation in the density and the surface tension. In addition, an increase in the contact angle (CA) of the ink droplet on the glass substrate was observed with increasing viscosity, as shown in Figure S5, Supporting Information.

From the rheological properties, a set of dimensionless constants, including Reynolds (Re), Weber (We), and inverse Ohnesorge (Z) numbers can be calculated and are used to determine the ink jettability.<sup>[21,22]</sup>

$$\text{Re} = \frac{\rho v l}{\eta} \quad (1)$$

$$\text{We} = \frac{\rho v^2 l}{\gamma} \quad (2)$$

$$Z = \frac{1}{\text{Oh}} = \frac{\text{Re}}{\sqrt{\text{We}}} = \frac{\sqrt{\rho l}}{\eta} \quad (3)$$

where  $\gamma$ ,  $\eta$ , and  $\rho$  are the surface tension, dynamic viscosity, and density of the ink, respectively.  $v$  is the droplet velocity.  $l$  is the characteristic length (i.e., nozzle orifice size of 21.5  $\mu\text{m}$ ), and Oh is the Ohnesorge number. The Z number has been identified as a key parameter. Low Z values indicate that the ink viscosity is too high to be ejected by the nozzle, while high Z values indicate a nonsufficient ink viscosity which leads to many satellite droplets.<sup>[23]</sup> A range of  $1 < Z < 10$  was proposed to be suitable for jetting.<sup>[21]</sup> Moreover, two additional constraints have to be considered. The first is a minimum We value of 4 to ensure sufficient energy for droplet ejection.<sup>[21]</sup> The other constraint,  $\text{We}^{1/2} \text{Re}^{1/4} > 50$ , is the threshold for the onset of droplet splashing upon ejecting on the substrate.<sup>[24]</sup> With all the aforementioned constraints, a map in the We–Re space can be constructed, as shown in Figure 1b. The white region in the middle indicates the printable region. In addition, the SU-8 inks listed in Table 1 are plotted in this map, where each solid line represents the jettability of one ink at different ejection velocities. It can be seen that Ink-30 and Ink-35 are too viscous and thus are outside of the printable region, whereas all other inks are within the printable region. The printability of the inks was further validated experimentally. Stable droplet ejection was possible with Ink-10, Ink-15, Ink-20, and Ink-25. In contrast, the droplet ejection was not stable with Ink-30 and there was no droplet ejection with Ink-35, as can be seen in Movie S2, Supporting Information. Therefore, an upper limit of the SU-8 concentration of below 30% was defined to ensure stable droplet ejection.

The lower limit of the SU-8 concentration is constrained by the UV-curing process. With the increasing concentration of the reactive diluent, a higher UV-exposure dose is needed. Using the methods described in Experimental Section, it was found that Ink-10 and Ink-15 are not curable with 385 nm due to the low amount of SU-8. As for the other two printable inks, Ink-25 needs much less UV exposure time (3 min) than Ink-20 (10 min). In addition, the ink materials' refractive indices and extinction coefficients in the wavelength range of 400 to 1200 nm were measured as a thin film by spectroscopic ellipsometry, and the results are shown in Figure 1c. The refractive indices decrease with increasing wavelength and become more similar to the glass's refractive index. Besides, the extinction coefficients of light above 400 nm are minimal and thus lead to low optical losses. The Ink-25 film shows a slightly higher refractive index than Ink-20, and at the same time, lower light loss occurs with Ink-25 film. Therefore, the further study in this work was carried out with Ink-25, and the term "ink" in the following texts refers to Ink-25.

**Table 1.** Rheological parameters of SU-8 inks in different concentrations.

Ink	SU-8 wt.%	Density [g cm <sup>-3</sup> ]	Surface tension [mN m <sup>-1</sup> ]	Viscosity @ 40 °C [mPa·s]	Ink validity
Ink-10	10%	1.0850 $\pm$ 0.0017	35.99 $\pm$ 0.18	13.96 $\pm$ 0.16	Not curable
Ink-15	15%	1.0893 $\pm$ 0.0058	35.48 $\pm$ 0.21	14.69 $\pm$ 0.07	Not curable
Ink-20	20%	1.0907 $\pm$ 0.0012	35.06 $\pm$ 0.12	16.61 $\pm$ 0.05	Printable, curable
Ink-25	25%	1.0963 $\pm$ 0.0085	34.51 $\pm$ 0.16	23.35 $\pm$ 0.06	Printable, curable
Ink-30	30%	1.0997 $\pm$ 0.0039	34.65 $\pm$ 0.35	30.34 $\pm$ 0.08	Not printable
Ink-35	35%	1.1101 $\pm$ 0.0073	35.50 $\pm$ 0.22	40.15 $\pm$ 0.09	Not printable

The fabrication process of MLAs with different NAs is illustrated in Figure 1d. First, a SAM film is formed on the glass substrate by spin coating. In this work, four different types of silanes, that is, 3-aminopropyltriethoxysilane (APTES), triethoxyphenylsilane (TEPS), trimethoxy-(3,3,3-trifluoropropyl)silane (TTFPS), and triethoxyoctylsilane (TEOS), were used for demonstration. Those molecules were chosen due to the large variety of their surface-free energy (SFE). As the right side of Figure 1d shows, each silane consists of three anchor groups and one customizable side chain, which can be modified to adjust the resulting SFE of the substrate.<sup>[25]</sup> The different SFEs then lead to different static CAs of the ink droplet on the treated substrate, where the CA rises from 13.0° on APTES to 40.4° on TEOS. It is worth mentioning that there are more silanes that can be used to decrease the SFE to even lower values than TEOS, and thus the aspect ratio of the lenses can be potentially tuned even further. After the SAM deposition, the MLAs are printed directly on the surface. This is followed by UV curing and a post-exposure baking process.

## 2.2. Automated Evaluations of the Printed MLAs

The microscope image of a printed MLA in a square layout is shown in Figure 2a. As can be seen, the MLA shows a very high uniformity in shape and alignment. The transmittance spectrum of such an MLA can be found in Figure S6, Supporting Information. Besides, the atomic force microscopy (AFM) image of a small area on an ML can be found in Figure S7, Supporting Information. The surface of the inkjet-printed MLs

is very smooth, which is indicated by the RMS roughness of 300 pm. Figure 2b shows the 3D surface profile of four MLs measured by confocal microscopy.

To evaluate the MLAs quantitatively and with meaningful statistics, the printed MLAs were then assessed with a custom-developed automated evaluation process.<sup>[26]</sup> The sag height information of the MLs can be extracted from the 3D optical profile of MLAs, as can be seen in Figure 2c. The algorithm estimated the tilt of the sample substrate surface caused by the slight tilt of the microscope stage. The profile image was then de-tilted and zero-leveled. The sag height values were then calculated by measuring the local maxima. The radii of the MLs were evaluated using the light microscope images. To obtain a global estimation of the radii of the MLs, the edges are detected using the Canny algorithm. The closed regions of the MLs are subsequently filled using a morphological fill, as shown in Figure 2d. Using 1D sections of the filled binary image, a radius estimation is obtained. This estimation is then used to bootstrap a subsequent multi-scale Hough transform to determine the precise center and radius of each ML individually. The sag heights and radii of the MLs printed on differently treated surfaces are shown in Figure 2e. The SFE of the substrate is adjusted by the choice of the SAM. When the SFE decreases, the radius of the ML decreases from 40.50 ( $\pm 1.02$ )  $\mu\text{m}$  to 26.72 ( $\pm 0.51$ )  $\mu\text{m}$ , while the sag height increases from 3.36 ( $\pm 0.13$ )  $\mu\text{m}$  to 8.80 ( $\pm 0.08$ )  $\mu\text{m}$  as the deposited ink volume was kept constant. The standard deviations of the radii are below 1.02  $\mu\text{m}$ , and of the sag heights are less than 0.13  $\mu\text{m}$ . On APTES, MLs with the smallest aspect ratio (0.08), which is defined as the ratio of the ML sag height over the radius,<sup>[27]</sup>

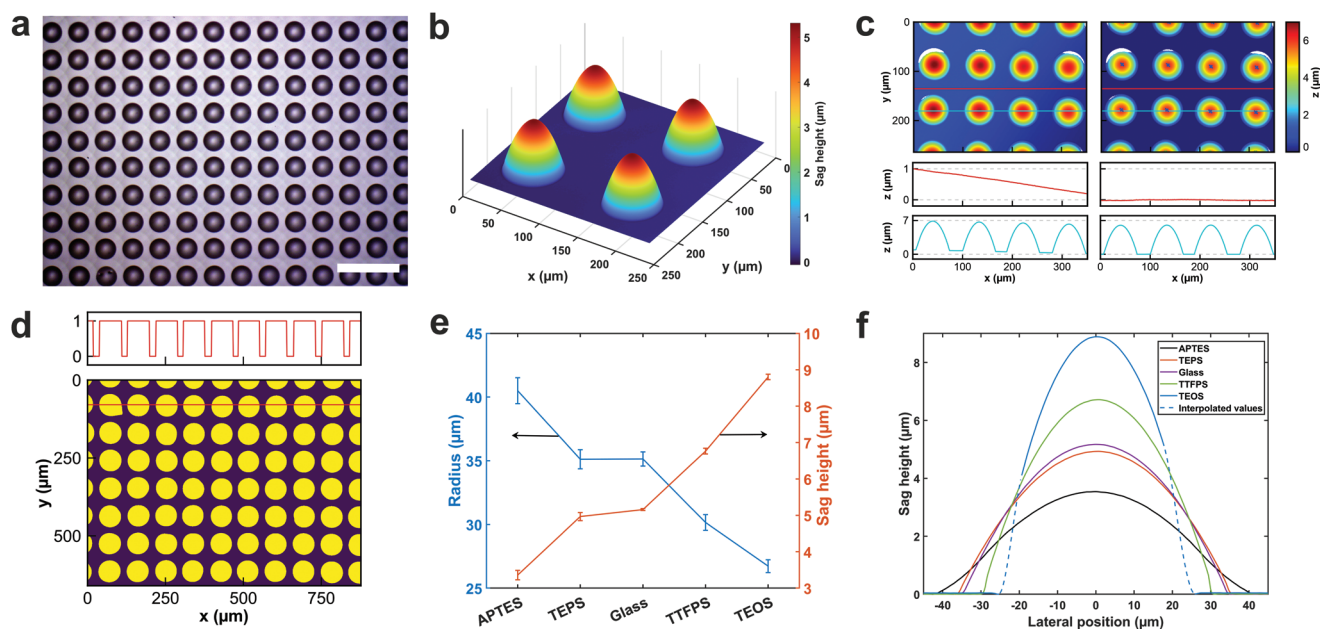


**Figure 2.** a) The microscope image of an MLA arranged in a square layout. Scale bar: 200  $\mu\text{m}$ . b) The surface profile of four MLs measured by confocal microscopy. The color bar on the right side indicates the sag height range of the MLs. c) First row: 3D optical profile images of an MLA. Second and third rows: height profiles corresponding to the red and blue paths in the first-row images. Left: original image. Right: de-tilted and zero-leveled image. d) Evaluation of the radii of the MLs. Lower: Filled binary image with maximum radius evaluation after edge detection via Canny algorithm. Upper: Binary profile of the red line indicated in the lower image. e) Radii (blue) and sag heights (red) of the MLs printed on differently treated substrates. The error bar represents the standard deviation for more than 100 MLs. Fine-tuning of the values is possible by mixing two silanes. f) The profiles of the MLs printed on differently treated substrates.

can be obtained, while a relatively high aspect ratio (0.33) was achieved by using TEOS as SAM film. Considering that only four silanes have been studied in this work and the wide variety of other silanes can be used for SFE tuning, it is possible to fabricate MLs with a specific aspect ratio by choosing an appropriate silane. Higher aspect ratios can be achieved using silanes which lead to lower SFEs than TEOS. Furthermore, fine-tuning the aspect ratio is also possible by mixing two silanes for the SAM.<sup>[28]</sup> The fine-tuning of the SFE by using a binary mixture of TTFPS and TEOS can be seen in Figure S8, Supporting Information. The profiles of the printed MLs on differently treated substrates are shown in Figure 2f. The profiles were reconstructed from the 3D optical profile images.

### 2.3. Fabrication of High-FF MLAs

In order to reach a higher FF, MLAs were printed in a hexagonal layout, as presented in Figure 3a. To realize the minimal gaps between MLs, the MLAs were printed in two runs. A scheme of the printing paths can be found in Figure S9, Supporting Information. First, the MLs in every other horizontal line were printed and UV-cured in situ. Subsequently, the other half of the MLA was printed following the same process. The UV-pinning constrains the overflow of the first half MLA droplets, and therefore merging effects are much less prominent in the printing of high-FF MLA. Figure 3b illustrates the geometry of a hexagonal MLA, and the FF can be calculated following the equation:

$$FF = \frac{2\pi r^2}{\sqrt{3}P \cdot P} \quad (4)$$

where  $r$  is the ML radius and  $P$  is the lateral pitch of the MLA, that is, the distance between the centers of two neighboring MLs. The radius  $r$  of the MLs on the glass substrate is  $35.14 (\pm 0.55) \mu\text{m}$ . The minimum pitch  $P$  that we have reached was  $71.35 \mu\text{m}$  with a printing resolution of 356 dpi. Accordingly, we achieved a record FF of 88% of inkjet-printed MLAs in a fast and straightforward way. Figure 3c shows the 3D surface profile of multiple MLs in the hexagonal MLA. Figure 3d is the scanning electron microscopy (SEM) image of the hexagonal MLA, and the high uniformity of the peripheral regions of the array can be seen.

### 2.4. Characterization of the Focal Lengths and Imaging Capability of the Printed MLAs

The focal length is a crucial parameter of an ML. The schematic of the setup for measuring the focal length is depicted in Figure 4a. The measurement was carried out using a collimated light source. The MLAs were mounted on a motorized precision linear stage driven with an accuracy of  $1 \mu\text{m}$ . The convex side of the MLAs was facing towards the camera. An objective lens and a CCD camera were used to magnify and obtain the images. All components were aligned to the same optical axis. During the measurement, the stage was first moved to the position where the plane side of the MLA was in focus. The MLA was then moved further away from the camera to image the focal plane of the MLA. In the case of a plano-convex thin lens, the relation between the focal length and the radius of curvature is given by the following equation:<sup>[29]</sup>

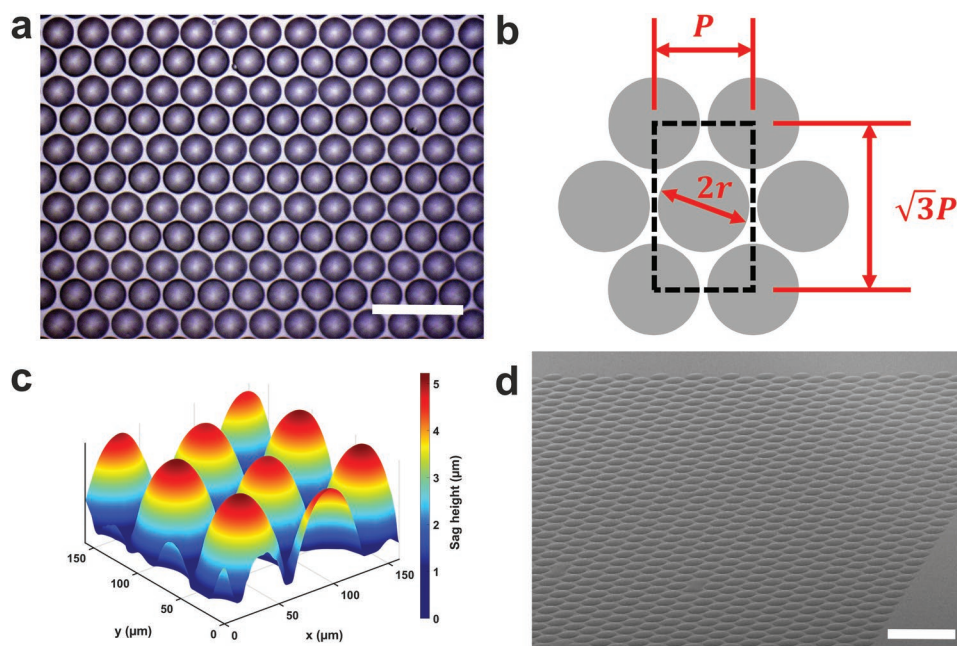


**Figure 3.** a) The microscope image of an MLA in a hexagonal layout. Scale bar:  $200 \mu\text{m}$ . b) The 2D geometrical model used for the calculation of the FF with a hexagonal layout.  $P$  stands for the pitch between two neighboring MLs in the lateral direction, and  $r$  is the radius of the MLs. c) The 3D surface profile of the printed MLA in a hexagonal layout. The color bar on the right side indicates the sag height range of the MLs. d) The SEM image of a corner of a hexagonal MLA. Scale bar:  $200 \mu\text{m}$ .

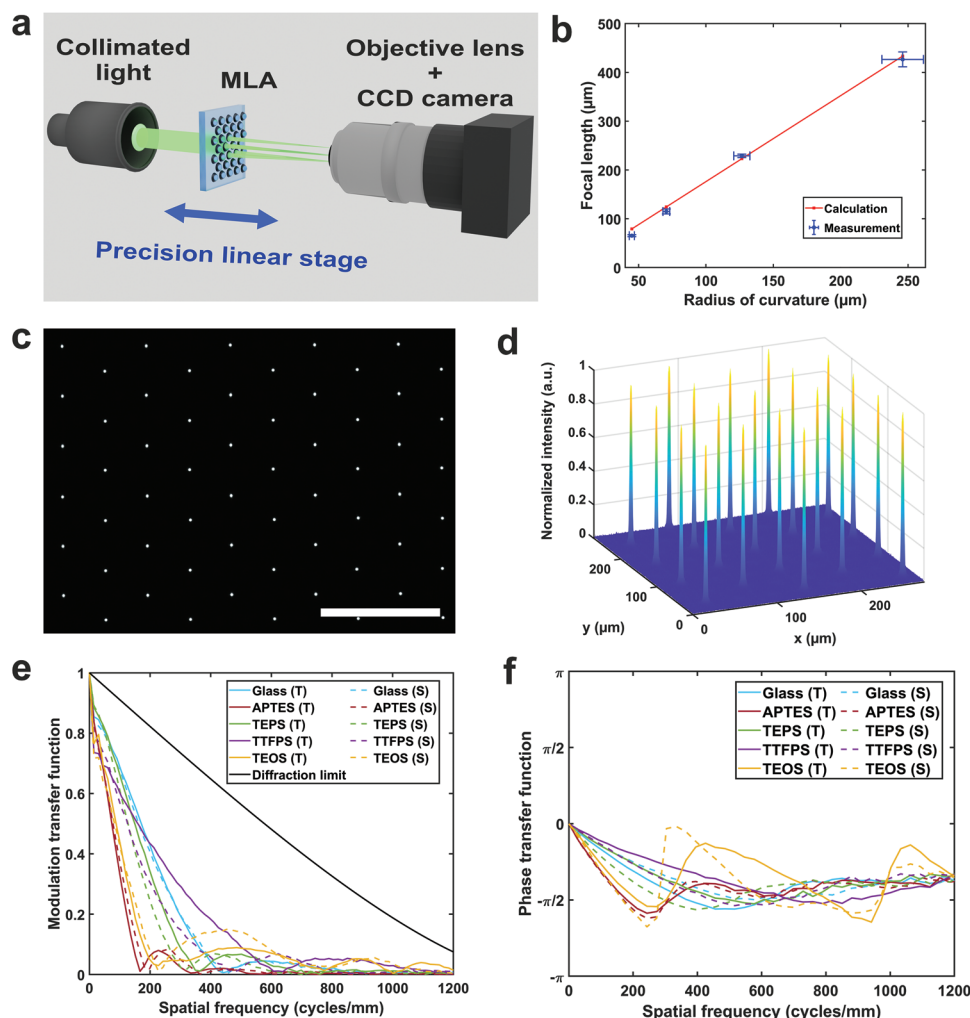


**Figure 4.** a) The focal length measurement system for the MLAs. b) The measured focal lengths (blue symbols with error bars) are compared to the calculated focal lengths (red line) with respect to the radius of curvature of the MLs. The error bars represent the measurement errors. c) The image of the focal plane. Scale bar: 100  $\mu\text{m}$ . d) The normalized intensity distribution of the light on the focal plane. e) The calculated tangential (T) (solid lines) and sagittal (S) (dashed lines) on-axis MTFs of the MLAs on differently-treated substrates. The diffraction limit in the figure represents the theoretical diffraction limit with the highest NA (0.38). f) The PTFs of the MLs on differently-treated substrates.

$$f = \frac{R}{n-1} \quad (5)$$

where  $f$  is the focal length,  $R$  is the radius of curvature, and  $n$  is the refractive index of the lens. Assuming the ML has a shape of a spherical cap solely caused by the substrate-ink interaction due to the surface tension,<sup>[21]</sup> the radius of curvature can be calculated as:

$$R = \frac{r^2}{2h} + \frac{h}{2} \quad (6)$$

where  $r$  is the radius of the microlens and  $h$  is the sag height of the microlens. From the values obtained from the automated evaluation (see Figure 2), the theoretical values of the focal length can therefore be calculated. The measured focal lengths and the calculated values are plotted in Figure 4b. Using the four different silanes, the focal lengths range from

65.3 to 426.7  $\mu\text{m}$ . The NA can be calculated using the following expression:<sup>[30]</sup>

$$\text{NA} = n_0 \sin \theta = n_0 \sin \left( \arctan \left( \frac{r}{f} \right) \right) \quad (7)$$

where  $n_0$  is the refractive index of the surrounding medium and  $\theta$  is the half-maximum angle of light acceptance. The results can be seen in Figure S10. Accordingly, an NA of approximately 0.09 was achieved by printed MLAs on APTES and the value increases to 0.38 on TEOS. Figure 4c shows the focal plane image of the MLA, and the intensity distribution of the focused light spots on this plane is presented in Figure 4d. It can be seen that on the focal plane, the light spots are uniformly distributed in a hexagonal pattern. Moreover, the intensity peaks have equal heights and are evenly distributed in space.

In order to quantitatively characterize the imaging performance of the printed MLAs, the on-axis optical transfer

functions (OTFs) were calculated based on the measured point spread function.<sup>[31]</sup> The amplitude of the OTF, that is, the modulation transfer function (MTF), in both tangential (T) and sagittal (S) planes are shown in Figure 4e. To take the MLA on the glass substrate as an example, the MTFs curves on the T and S planes are very close to each other, which indicates very low aberrations caused by asymmetry, such as astigmatism of the lenses. In addition, using the calculated NA values of the MLs, a comparison of the measured MTF and the theoretical MTF for the individual microlenses can be found in Figure S11. As can be seen, the MTFs of different MLAs are all beyond 0.5 until the spatial frequency of 50 cycles/mm, indicating a high-performance imaging quality of the MLAs. Moreover, the phase transfer function (PTF), which is the phase of the OTF, was also calculated for different MLs, and the results are shown in Figure 4f. The PTF presents the asymmetrical aberrations and poor centering of elements.<sup>[29]</sup> For an ideal and aberration-free lens, the PTF is zero for all spatial frequencies and in all directions. The absolute PTF values of the microlenses are all below  $\pi/4$  until 50 cycles  $\text{mm}^{-1}$ , which also indicates a good imaging quality.

To have a more intuitive impression of the imaging capability of the MLA, some letters and patterns were imaged directly by the printed MLAs. A similar optical setup was used, in which the collimated light source was replaced by an illuminated object, as shown in Figure 5a. When the object was a word “MLA”, the real image containing an array of “MLA”s was captured by the CCD camera, as can be seen in Figure 5b. The excellent image quality and the uniform distribution of the miniaturized ‘MLA’s again indicate the high quality of the fabricated MLA. Furthermore, when a square grid replaced the letters, as shown in Figure 5c, a clear and uniform image can still be obtained through the MLA. The undistorted grids on the sensor further indicate that the printed MLA has outstanding geometrical and optical properties.

## 2.5. Fabrication of MLAs on Large and Flexible Substrates

A vital advantage of the inkjet printing approach is the capability for large-scale fabrication of MLAs. In addition, a customized large area fabrication by printing, either in the form of letters or arbitrary patterns, is possible. Two logos were printed on a 10 cm  $\times$  10 cm glass substrate, as shown in Figure 6a. The printed MLAs clearly display the defined patterns. Furthermore, our approach can be transferred to flexible substrates. To demonstrate the flexibility and feasibility of the inkjet-printed MLAs, MLAs were directly printed on polydimethylsiloxane (PDMS) substrates, as shown in Figure 6b,c. The microlenses were printed on a 10 cm  $\times$  4 cm PDMS band, and the band can be easily twisted and bent. The microscope image of the MLA printed on pristine PDMS is shown in Figure S12, Supporting Information.

## 2.6. Discussion

With the method proposed in this paper, we have successfully fabricated MLAs with a high FF and high uniformity by direct inkjet printing. The ink and the printing parameters have been optimized so that the jetting process is very stable and free of satellite droplets. Therefore, the uniformity of the printed MLAs in terms of both the shape of each microlens and the alignment of the array has been improved to a large extent. Based on the quantitative evaluations of the printed MLAs, the standard deviations of the radii were below 2.5%, and of the sag heights were less than 3.9%. Besides, due to the very low solvent concentration in the ink, there is only a small volume shrinkage or drying effects of the microlenses after curing. Hence, the spacings between microlenses can be reduced drastically, and a high FF can be achieved. Furthermore, with the

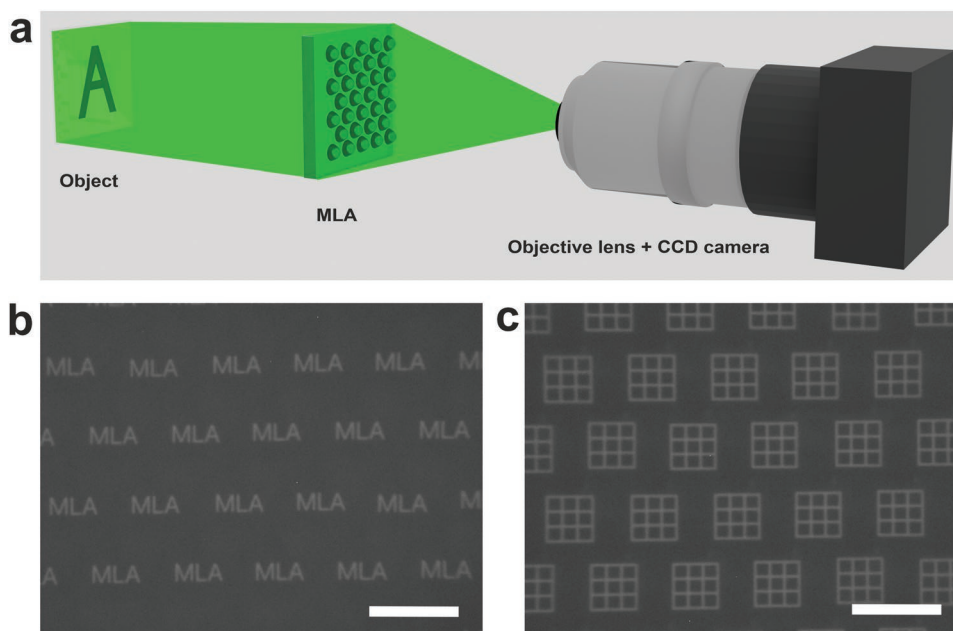


**Figure 5.** a) The optical imaging system for the MLAs. b) The image of the word “MLA”. Scale bar: 100  $\mu\text{m}$ . c) The image of a square grid. Scale bar: 100  $\mu\text{m}$ . The objects have a height of  $\approx 5$  cm.

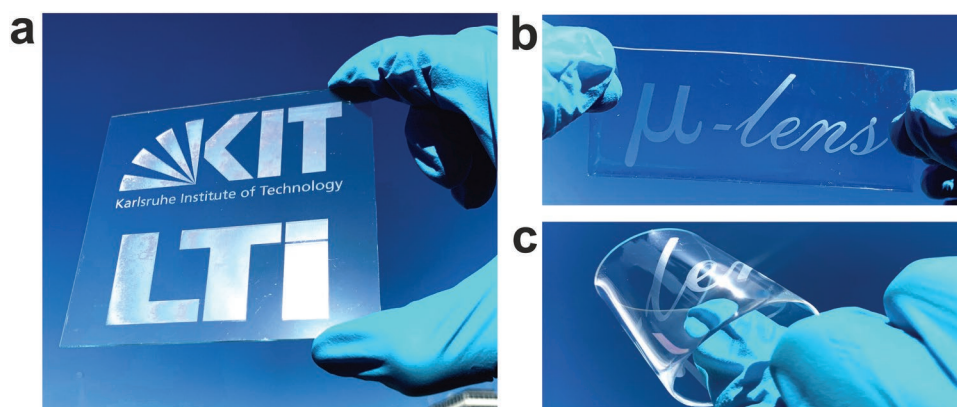


**Figure 6.** a) The image of the MLA printed on a large glass substrate. Size of the substrate: 10 cm × 10 cm. The MLA is printed in the pattern of the logos of the institutes. b) The image of the MLA printed on a PDMS substrate. Size of the substrate: 10 cm × 4 cm. The substrate is flattened. c) The image of the MLA printed on a PDMS band. The PDMS band is twisted and bent.

accurate positioning of microlenses and the instant in situ UV curing process, closely-packed MLAs in a hexagonal layout have been fabricated. Therefore, our approach provides a straightforward and fast method for fabricating uniform MLAs with FFs of up to 88% without surface pre-structuring steps. Additionally, the aspect ratio of the microlenses can be easily controlled by utilizing different SAMs, which adjust the SFE of the substrate.<sup>[32]</sup> Due to the commercial availability of a wide range of silanes, there are various options for tuning the aspect ratio and thus the NA of the MLs. Furthermore, it can also lead to the substrate-independent fabrication of MLAs,<sup>[25]</sup> and hence the fabrication process can be easily transferred to various substrates, for example, flexible foils. Moreover, larger lenses can be easily fabricated either by depositing multiple droplets for a single ML, as shown in Figures S13 and S14, Supporting Information, or by using print heads with a higher droplet volume.

### 3. Conclusion

We have demonstrated the fabrication of MLAs by inkjet printing. The FF of the fabricated MLAs can reach 88% by using a modified SU-8 ink and in situ UV-curing. Different NAs of microlenses have been obtained by applying different SAMs on the substrate. Using the four selected silanes, the NA can be tuned from 0.09 to 0.38. The printed MLAs show outstanding uniformity and excellent imaging performance. With the developed ink and printing process, MLAs can be fabricated in a simple, cost-effective, and flexible manner, allowing for customized patterns, different sizes, and mass production. It is also possible to print MLAs on both rigid and flexible substrates or even directly on top of optoelectronic devices, for example, photodiodes and light-emitting devices, thus opening a wide range of integration possibilities and applications.

### 4. Experimental Section

**Substrate Preparation:** The 22 mm × 22 mm borosilicate glass substrates (Carl Roth) and the 10 cm × 10 cm glass substrate were cleaned in an ultrasonic bath with acetone and then with isopropyl

alcohol for 10 min each. The substrates were dried with nitrogen after each step. These substrates were used as untreated glass substrates in this work. Furthermore, different SAM substrates were prepared as described in the previous work.<sup>[25]</sup> In this work, four different SAM-treatments were investigated: 3-aminopropyltriethoxysilane (APTES) (Acros Organics 99%), triethoxyphenylsilane (TEPS) (Sigma-Aldrich > 98%), trimethoxy-(3,3,3-trifluoropropyl)-silane (TTFPS) (Sigma-Aldrich ≥ 97.0%), and triethoxyoctylsilane (TEOS) (Sigma-Aldrich 98%). The flexible PDMS substrate was prepared by first mixing a pre-polymer base of PDMS Sylgard 184 silicone elastomer (Dow Corning) with its cross-linking curing agent in a 10:1 mass ratio.<sup>[33]</sup> The thoroughly stirred mixture was degassed in a vacuum desiccator for 30 min. Subsequently, the degassed mixture was poured onto a clean glass plate and cured on a hotplate at 100 °C for 30 min. The PDMS substrate was then carefully peeled from the glass plate.

**Ink Formulation and Inkjet Printing:** The inks consist of SU-8 2150 (Kayaku Advanced Materials) diluted in reactive diluent Erisys GE-20 (Huntsman) with a concentration of 10, 15, 20, 25, 30, and 35 wt.% for Ink-10, Ink-15, Ink-20, Ink-25, Ink-30, and Ink-35, respectively. The reference ink Ink-Cyclopentanone (SU-8 with non-reactive diluent) consists of SU-8 2150 (Kayaku Advanced Materials) diluted in cyclopentanone (Sigma-Aldrich ≥99%) with a concentration of 25 wt.%.

Before printing, the ink was placed in an ultrasonic bath for degassing for 10 min and then filtered using PTFE filters with a pore size of 0.2 μm. The inkjet printer (PixDro LP50) was equipped with a 10 pL cartridge (Fujifilm Dimatix). The jetting frequency was kept at 1 kHz during printing, and a customized jetting waveform was designed to obtain satellite-free droplets at this frequency. During printing, one nozzle was used for jetting. The print head temperature was set to 32 °C, and the printing platform temperature was kept at 24 °C. After each printing run, the MLA was exposed at 40 °C under a UV-LED (Hamamatsu) with a central wavelength of 385 nm for 3 min. For the fabrication of high-FF MLAs, the UV curing time was doubled to 6 min due to two printing runs. The cross-linking process was completed with a subsequent post-exposure bake at 95 °C on a hotplate for 10 min. The resolution of the printing recipe determines the pitch between microlenses, and the resolutions were 320 dpi × 320 dpi for the square layout of the MLA and 356 dpi × 278 dpi for the hexagonal layout. The entire fabrication process was completed in a cleanroom, where the ambient temperature was at 21–22 °C, and the humidity was at 40–50%. The minimum exposure time of the inks was determined using the UV-LED (Hamamatsu). After printing, the MLAs were exposed at 40 °C under UV for different time durations. Afterwards, the MLAs were post-exposure baked at 95 °C for 3 min. Subsequently, the MLAs were rinsed in the SU-8 developer (MicroChem) for 1 min. The MLAs were considered cured when the structures were not washed after development. Besides, the MLAs were considered as not curable if they were not cured after 1 h of UV exposure.

**Characterization:** The complex refractive indices of the ink materials were determined utilizing spectroscopic ellipsometry (VASE ellipsometer, J.A. Woollam) and processed in the ellipsometric analysis program WVASE (J.A. Woollam). The surface tension of the inks, the static CAs of the ink on differently treated substrates, and the video of the inks' volume shrinkage in ambient conditions was measured or recorded by a CA measuring system (OCA 50, DataPhysics Instruments) under ambient conditions. The viscosity of the inks was measured by a viscometer (m-VROC, RheoSense). The microscope images of the MLAs were taken by a light microscope (Axioplan 2 imaging, Carl Zeiss) equipped with a CCD camera (AxioCam ICc3, Carl Zeiss). The 3D optical profiles of the MLAs in a square layout were obtained using a 3D optical surface metrology system (Leica DCM8). The 3D optical profiles of the MLAs in the hexagonal layout, the profiles of the printed thin films in the coffee-stain effect comparison, and the profiles of the printed droplets in the volume shrinkage study were measured by a 3D optical profilometer (ContourGT-X, Bruker). The surface morphology was measured by AFM (NanoWizard, Bruker Nano), and the surface RMS roughness was analyzed with Gwyddion. The SEM images were taken by SUPRA 55 (Carl Zeiss) at 5 kV. The focal length measurement was completed using a collimated LED light source at 530 nm (M530L4-C4, Thorlabs), a precision linear stage (Owis), a 60× objective lens (NA 0.85), and a CCD camera. And the 60× objective lens was replaced by a 40× objective lens in the imaging test. The transmittance spectrum was measured with a spectrophotometer (Lambda 1050+ UV/VIS/NIR, PerkinElmer) with an integrating sphere module.

## Supporting Information

Supporting Information is available from the Wiley Online Library or from the author.

## Acknowledgements

The authors gratefully acknowledge the Deutsche Forschungsgemeinschaft (DFG, German Research Foundation) under Germany's Strategy via the Excellence Cluster 3D Matter Made to Order (3DMM2O, EXC-2082/1-390761711) and the Baden-Württemberg Stiftung gGmbH for financial support (30001027/28). The authors also acknowledge support from the Bundesministerium für Bildung und Forschung (BMBF) through ForLab (16ES0948).

Open access funding enabled and organized by Projekt DEAL.

## Conflict of Interest

The authors declare no conflict of interest.

## Data Availability Statement

The data that support the findings of this study are available from the corresponding author upon reasonable request.

## Keywords

additive manufacturing, inkjet printing, microlens arrays, UV-curable ink

Received: March 22, 2022

Revised: May 1, 2022

Published online: June 13, 2022

- [1] a) P. Gorzelak, M. A. Salamon, R. Lach, M. Loba, B. Ferré, *Nat. Commun.* **2014**, *5*, 3576; b) S. Petsch, S. Schuhlraden, L. Dreesen, H. Zappe, *Light: Sci. Appl.* **2016**, *5*, e16068; c) J. Yong, H. Bian, Q. Yang, X. Hou, F. Chen, *Front. Chem.* **2020**, *8*, 883.
- [2] I. Sachs, M. Fuhrmann, I. Verboven, I. Basak, W. Deferme, H. Möbius, *Adv. Eng. Mater.* **2021**, *23*, 2100212.
- [3] a) B. P. Keyworth, D. J. Corazza, J. N. McMullin, L. Mabbott, *Appl. Opt.* **1997**, *36*, 2198; b) B. Stoklasa, L. Motka, J. Rehacek, Z. Hradil, L. L. Sánchez-Soto, *Nat. Commun.* **2014**, *5*, 3275.
- [4] C. Fang, J. Zheng, Y. Zhang, Y. Li, S. Liu, W. Wang, T. Jiang, X. Zhao, Z. Li, *ACS Appl. Mater. Interfaces* **2018**, *10*, 21950.
- [5] S.-I. Bae, K. Kim, K.-W. Jang, H.-K. Kim, K.-H. Jeong, *Adv. Opt. Mater.* **2021**, *9*, 2001657.
- [6] J. Y. E. Chan, Q. Ruan, R. J. H. Ng, C.-W. Qiu, J. K. W. Yang, *ACS Nano* **2019**, *13*, 14138.
- [7] M. H. Wu, G. M. Whitesides, *Adv. Mater.* **2002**, *14*, 1502.
- [8] J. R. Leger, M. L. Scott, W. B. Veldkamp, *Appl. Phys. Lett.* **1988**, *52*, 1771.
- [9] a) H. M. Kim, M. S. Kim, G. J. Lee, Y. J. Yoo, Y. M. Song, *Opt. Express* **2019**, *27*, 4435; b) E. Wrzesniewski, S.-H. Eom, W. Cao, W. T. Hammond, S. Lee, E. P. Douglas, J. Xue, *Small* **2012**, *8*, 2647.
- [10] H. Jung, K.-H. Jeong, *ACS Appl. Mater. Interfaces* **2015**, *7*, 2160.
- [11] S. Surdo, R. Carzino, A. Diaspro, M. Duocastella, *Adv. Opt. Mater.* **2018**, *6*, 1701190.
- [12] R. Magazine, B. van Bochove, S. Borandeh, J. Seppälä, *Addit. Manuf.* **2022**, *50*, 102534.
- [13] N. Jürgensen, B. Fritz, A. Mertens, J.-N. Tisserant, M. Kolle, G. Gomard, G. Hernandez-Sosa, *Adv. Mater. Technol.* **2021**, *6*, 1900933.
- [14] X. Li, H. Tian, Y. Ding, J. Shao, Y. Wei, *ACS Appl. Mater. Interfaces* **2013**, *5*, 9975.
- [15] Y. Ding, Y. Lin, L. Zhao, C. Xue, M. Zhang, Y. Hong, S. Peng, W. Wen, J. Wu, *Adv. Mater. Technol.* **2020**, *5*, 2000382.
- [16] T. Gissibl, S. Thiele, A. Herkommer, H. Giessen, *Nat. Photonics* **2016**, *10*, 554.
- [17] a) B. J. deGans, P. C. Duineveld, U. S. Schubert, *Adv. Mater.* **2004**, *16*, 203; b) J. del Barrio, C. Sánchez-Somolinos, *Adv. Opt. Mater.* **2019**, *7*, 1900598; c) A. Teichler, J. Perelaer, U. S. Schubert, *J. Mater. Chem. C* **2013**, *1*, 1910.
- [18] a) D. Xie, H. Zhang, X. Shu, J. Xiao, *Opt. Express* **2012**, *20*, 15186; b) F. Vahid, M. Gregory, K. J. Yeon, M. Alcherio, B. Juergen, *Micro Nanosyst.* **2009**, *1*, 63; c) Y. Luo, L. Wang, Y. Ding, H. Wei, X. Hao, D. Wang, Y. Dai, J. Shi, *Appl. Surf. Sci.* **2013**, *279*, 36.
- [19] a) L. Jacot-Descombes, M. R. Gullo, V. J. Cadarso, J. Brugger, *J. Micromech. Microeng.* **2012**, *22*, 074012; b) M. Blattmann, M. Ocker, H. Zappe, A. Seifert, *Opt. Express* **2015**, *23*, 24525.
- [20] F. Ceysens, R. Puers, in *Encyclopedia of Nanotechnology* (Ed: B. Bhushan), Springer, Dordrecht, Netherlands **2012**, p. 2530.
- [21] B. Derby, *Annu. Rev. Mater. Res.* **2010**, *40*, 395.
- [22] H. Roh, D. Ko, D. Y. Shin, J. H. Chang, D. Hahm, W. K. Bae, C. Lee, J. Y. Kim, J. Kwak, *Adv. Opt. Mater.* **2021**, *9*, 2002129.
- [23] M. Robin, W. Kuai, M. Amela-Cortes, S. Cordier, Y. Molard, T. Mohammed-Brahim, E. Jacques, M. Harnois, *ACS Appl. Mater. Interfaces* **2015**, *7*, 21975.
- [24] C. D. Stow, M. G. Hadfield, J. M. Ziman, *Proceedings of the Royal Society of London. A. Mathematical and Physical Sciences* **1981**, *373*, 419.
- [25] S. Schliske, M. Held, T. Rödlmeier, S. Menghi, K. Fuchs, M. Ruscello, A. J. Morfa, U. Lemmer, G. Hernandez-Sosa, *Langmuir* **2018**, *34*, 5964.
- [26] M. Schambach, Q. Zhang, U. Lemmer, M. Heizmann, *tm – Technisches Messen* **2021**, *88*, 342.

- [27] J. Chen, B. Fritz, G. Liang, X. Ding, U. Lemmer, G. Gomard, *Opt. Express* **2019**, 27, A25.
- [28] X. Bulliard, S.-G. Ihn, S. Yun, Y. Kim, D. Choi, J.-Y. Choi, M. Kim, M. Sim, J.-H. Park, W. Choi, K. Cho, *Adv. Funct. Mater.* **2010**, 20, 4381.
- [29] E. Hecht, *Optics*, Addison-Wesley, Reading, MA **2002**.
- [30] B. Qin, X. Li, Z. Yao, J. Huang, Y. Liu, A. Wang, S. Gao, S. Zhou, Z. Wang, *Opt. Express* **2021**, 29, 4596.
- [31] F. Liu, Q. Yang, F. Chen, F. Zhang, H. Bian, X. Hou, *Opt. Lett.* **2019**, 44, 1600.
- [32] a) A. Ulman, *Chem. Rev.* **1996**, 96, 1533; b) J. Y. Kim, K. Pfeiffer, A. Voigt, G. Gruetzner, J. Brugger, *J. Mater. Chem.* **2012**, 22, 3053.
- [33] Q. Jin, Q. Zhang, J. Chen, T. Gehring, S. Eizaguirre, R. Huber, G. Gomard, U. Lemmer, R. Kling, *Adv. Mater. Technol.* **2021**, 7, 2101026.